Review

Coating of bioactive glass on magnesium alloys to improve its degradation behavior: Interfacial aspects

V.S. Yadav[a], M.R. Sankar[a,b,c,*], L.M. Pandey[a,d,*]

[a] Centre for the Environment, Indian Institute of Technology Guwahati, Assam, 781039, India
[b] Department of Mechanical Engineering, Indian Institute of Technology Guwahati, Assam, 781039, India
[c] Department of Mechanical Engineering, Indian Institute of Technology Tirupati, Andhra Pradesh, 517506, India
[d] Department of Biosciences and Bioengineering, Indian Institute of Technology Guwahati, Assam, 781039, India

Abstract

The preferable mechanical properties of Mg alloys along with excellent compatibility with human bone have established their applicability as implant biomaterials. However, a higher corrosion/degradation rate of Mg alloys in body fluids limits its biomedical applications. In this direction, surface modification and coating are explored as appropriate strategies to mode the degradation rate of Mg alloys. The constituents of bioactive glass (BG) provide strength, bio-inertness and bone bonding capability. Hence, researchers have explored the coating of BG on Mg alloys and investigated chemical, mechanical and biological properties of the coated alloys. In this review, we have made an attempt to compile the literature works done on the coating of BG on Mg alloys and its features. Underlying interfacial aspects of the coated substrates towards the degradation behavior are highlighted. The way forward to further improve the coating characteristics of BG coated Mg alloys are remarked.

1. Introduction

The use of metallic implants can be traced early back in 18th centuries when it was used for injured defense personals in war by English speaking nations. But to the mid of the nineties, it got an end to this use. However, the industrial revolution back in the nineties increased technological advances and reinstated its need for various orthopaedic applications. Primarily it was used for bone repair and fracture fixation of short and long bones. Though, little attempt was made for the complete replacement through implant surgeries and supporting implants. Towards this, bone pins and spinal wires of iron, silver and gold had been first successfully used in the 1860s [1]. Afterwards, applications of metallic implants for orthopaedic surgery have expanded in the medical industry. Various researches for the improved applications of metallic biomaterials started from the 20th century for the modern reconstruction surgery of hard tissues and organs. For example, Titanium used in surgical implants as hip ball, bone and dental implant [2–5], Stainless steel for surgical tools and implants, bone replacements and reinforcements [6], Nickel-Titanium [7] alloys as vascular stents [8,9], and magnesium Mg based alloys for bone regeneration and tissue engineering [10–12].

Even the large numbers of alloys available by manufacturers, only a few of them are found to be biocompatible, which is a desired feature for an implant material in the orthopaedic practices. These materials are broadly classified in the four classes based on their major alloying elements as shown in Fig. 1. Stainless steel, cobalt and titanium based alloys are being routinely applied as implants [13]; while miscellaneous

* Corresponding authors.
   E-mail addresses: vivek18c@iitg.ac.in (V.S. Yadav), evmrs@iittp.ac.in (M.R. Sankar), lalitpandey@iitg.ac.in (L.M. Pandey).
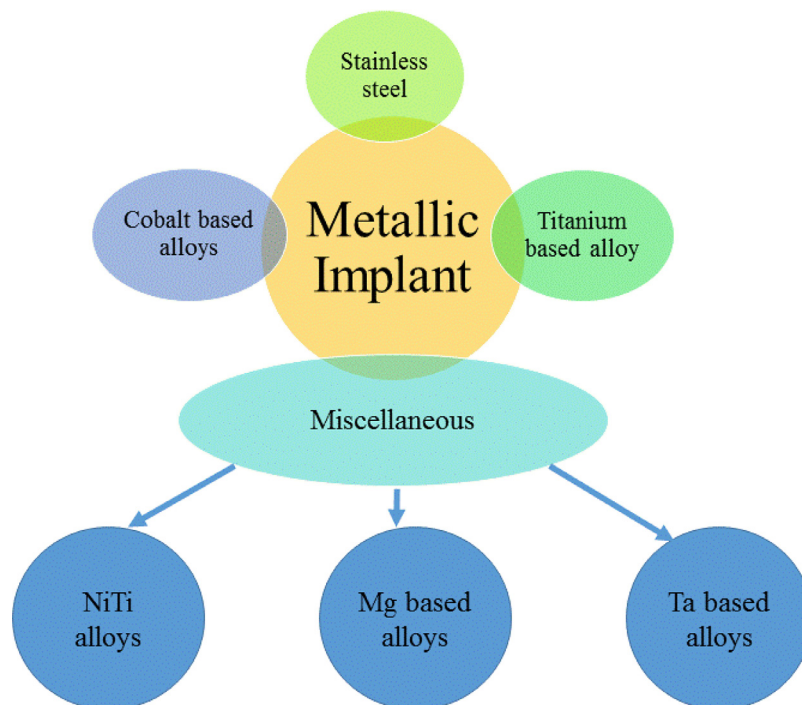
Fig. 1. Different classes of metallic biomaterials.

e.g. NiTi, Mg and Tantalum alloys are approved by the Food and Drugs Administration and are under clinical trials [14]. Recently, alloys of the last two categories, Ti and Mg, have proven there applicability in orthopedic surgeries along with biocompatibility. However, medical implants made by these alloys are yet to be routinely applied and continuous researches are going on in this direction. For example, Mg based alloys were recently tested *in-vivo* as biliary stents in rabbits [15,16].

The preferable mechanical properties and excellent compatibility of Mg alloys with human bone have proven their suitability as implant biomaterials [17]. Mg alloys have a moderate elastic modulus of 45 GPa close to the human bone (16–22 GPa) as compared to stainless steel (50 GPa) and Ti alloy (52 GPa) [7]. Further, the risk of osteoporosis is effectively decreased using Mg alloys because of the comparable density of $1.74\,g\,cm^{-3}$ (similar to bones 1.7–$2.1\,g\,cm^{-3}$) and stress-shielding effect to natural bone [18, 19]. In addition, Mg is generally present in the human body (25 g in an adult) in the bones and soft tissues [20]. It also has no noxiousness effect and any excess quantity is easily excreted by the body [21]. Furthermore, it participates in bone metabolism and found to stimulate the formation of new bone tissue [22].

During the degradation process, Mg alloys are found to offer a better reconstruction and repair of bone along with the minimum inflammatory responses [23,24]. However, as a resorbable biodegradable implant material, it is requisite that Mg alloys should persist inside the body and sustain their mechanical integrity over a period of 12–18 weeks similar to the healing of bone tissues. In other words, the degradation rate of the material should match with the bone healing rate

and eventually the material is completely swapped by natural tissue [25]. However, a higher corrosion/degradation rate of Mg alloys in blood plasma and human body fluid compromises its mechanical integrity, which in turn limits biomedical applications [16]. Therefore surface modification with appropriate coating on Mg alloys is considered as an effective technique to moderate the degradation rate [26]. Many researchers have tried to control the corrosion of magnesium alloys by bioactive glass coatings which have a similar composition to the bone and demonstrated superior bioactivities [27]. In this review, the coating of bioactive glass (BG) based bioceramics over Mg alloys and its effect on degradation behavior is mainly focused. The effect of various interfacial factors such as coating thickness surface wettability and surface pretreatment, towards adhesion strength and degradation potential/rate are discussed. Additionally, various coating techniques being used for this purpose are briefly summarized.

2. Bioactive glasses (BG): properties and coating

For a biomaterial, interfaces between biomaterial and host environment are an important area of interest, which majorly regulate the biocompatibility. These interactions decide the fate of a biomaterial to perform its intended function. In this regard, BG material had gained attention as a biomaterial in bone-regeneration applications. It has been successfully applied over a wide range of implant materials such as titanium [28], stainless steel [29] and magnesium alloys [30,31] for different orthopedic applications. These coating resulted in improved corrosion resistance, adhesion strength and bioactivity. The bone-bonding capability of BG is considered to be the
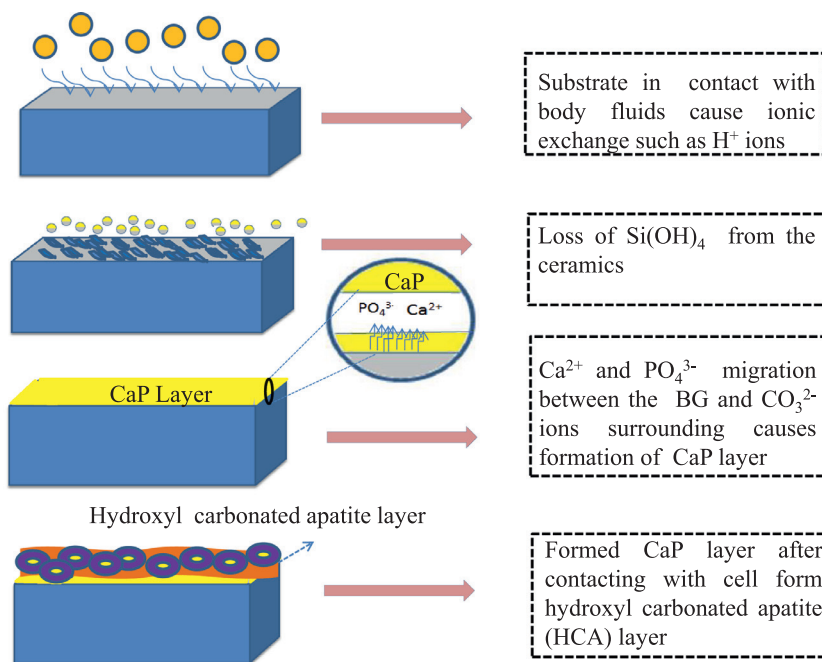
Fig. 2. *In-vitro* mechanism of action of BG coated substrates in SBF.

most significant properties for its material biocompatibility. It mainly contains silicon dioxide (≤ 52 wt%) as binding substance, sodium dioxide (≤ 32 wt%) as strength provider, calcium oxide (≤ 16 wt%) and phosphorus pentoxide (≤ 6 wt%) as bio-inerts for bone formation. Due to the presence of these components, BG is reported not only to bond with the bones, but also with soft tissue [23]. It offers a rapid rate of the surface activity causing uninterrupted and speedy attachment to aligning tissue through chemical bonding [32]. Mechanism of action of BG coated substrates in SBF is illustrated in Fig. 2. BG coated substrate releases alkaline or alkali elements replacing cations with H_3O^+ and H^+ from SBF. After which, dissolution of $Si(OH)_4$ through the action of hydroxyl ions takes place. Migration of calcium and phosphate ions and reaction with CO_3^{2-} ions present in SBF forms Calcium phosphate layer. In fact, bone bonding capability of bioglass is linked with its property to form a carbonated apatite layer [23].

The understandings of cell response to bioglass coated Mg alloys and other implant materials have driven researchers to further advance the properties of BG by creating its composite with polymers. In this regard, various advancements to bioactive glass have been discussed. Table 1 represents various methods to produce BG along with their compressive strength (C_s), tensile strength, porosity and pore size at different sintering temperatures for various intended biomedical applications. These methods includes chemical methods such as sol-gel, three stage preparation process (mixing, compression and calcination), gel casting method and other processes like polymeric sponge, foam replica, powder-metallurgy, robcast and lithography. Though physical processes have advantages of high compressive strength but the chemical process
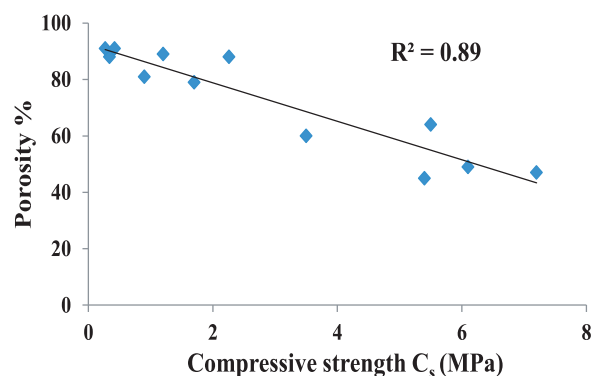
Fig. 3. The comparative trend between porosity and Compressive strength of different method produce bioactive glass (Data were taken from Table 1).

is quick, low cost and easily controlled. Physical properties of the coating are expected to affect the mechanical properties. We plotted porosity vs compressive strength C_s data from the literature (Table 1). C_s of the coating was found to be inversely proportional to porosity (Fig. 3). In fact, sintering temperature (T_s) is reported to inversely affect C_s i.e. $C_s = \frac{1}{T_s}$ [33]. To achieve a specific enhancement in the property, doping of metals is done as listed in Table 1. Doping of zinc helped in improving the toughness and hardness because of their tetrapod shaped structure [34,35], Copper, as an essential body substance is significant in angiogenesis and blood vessel maturation [36,37]. Whereas silver helped in imparting antibacterial property to the material [38]. Titanium reduced biological corrosion with good biocompatibility and improved hardness [39,40]. Further advancement in nanotechnology has demonstrated the effect on composition on its bulk proper-

Table 1
Various properties of BG, metal doped BG and their polymer composites for different biomedical applications.

Materials	Intended applications	Process	Compressive strength (C_s) /Tensile strength (MPa)	Porosity (%)	Sintering temperature °C	Other reported properties	Ref.
45S5	Bone tissue engineering application	Sol-gel	0.34 - 2.26	88–82	600–1000	Pore Size $=98\,\mu m$	[33]
45S5 foam	Bone tissue engineering	Polymer-sponge	0.27–0.42	91	1000	Pore Size $=510$–$720\,\mu m$	[45]
45S5	In clinical prosthesis	Produced by foam replication	1.2 ± 0.2	89	700	Weibull modulus of 6	[46, 47]
45S5 foam	Middle ear prosthesis	Powder metallurgy-foam technology	1.7 - 5.5	64 – 79	900	Pore Size $=335$ - $530\,\mu m$	[48]
45S5	Tissue engineering application	Three stage preparation mixing(in aqueous solution), compression, and calcination	5.4 – 7.2	45.9–47.2	1050	Pore size $=420\,\mu m$ in length $100\,\mu m$ in breadth Apparent density- 1.5 ± 0.3	[49]
45S5	Bone tissue engineering	Robcasting	6.1 ± 2.6	49.1 ± 5.5	600	Weibull modulus of 3, Fracture Energy- $93\,kJ/m^3$	[50]
45S5	Orthopedic application	Stereo lithographic	3.5 - 6.7	~ 60	950	Pore size $=400$- $700\,\mu m$	[51]
β-TCP–45S5 Bioglass	Dental and orthopedics applications	Gel casting method	0.9 ± 0.3	81.6 ± 0.6	1200	Pore size $=200$–$500\,\mu m$	[52]
Metal doped BG							
Cu-45S5	Bone tissue engineering application	Foam replica technique	0.2–0.3	90	1050	Pore size in the range of 200–$300\,\mu m$, Improved angiog-enesis function	[53]
Zn-45S5	Composite scaffolds in bone repair.	Sol-gel method	3.69 ± 0.30	87.0 ± 3.3	650	Pore size in the range of 100–$800\,\mu m$, Weibull modulus of 3, Improved hardness and showed good biocompatibility	[54]
Ti-45S5	Dental implant application	Mechanical alloying and powder metallurgy process	1.5	70	1300	Pore size $=150$- $500\,\mu m$	[55]
Ag-4545	Tissue engineering application	Sol-gel method	2.5	81	600	Pore size $=70$- $120\,\mu m$, Enhanced anti-bacterial property.	[38]
BG-polymer composites							
Chitosan −45S5 BG	For Guided tissue regeneration	solution casting method	$T_s = 38 \pm 2$	NA	NA	Young's modulus $=0.72 \pm 0.07$ GPa	[56]
Chitosan-45S5 BG Microsphere	For Guided tissue and bone regeneration	Solution casting method	$T_s = 25 \pm 2$	NA	NA	Young's modulus $=0.51 \pm 0.07$ GPa	[56]
Poly(L-lactic acid)−45S5	Orthopedic applications	Sol-gel and co-precipitation method	0.35	88.4	700	Pore Size $= 10$- $150\,\mu m$	[57]
Mesoporous BG doped-poly (3-hydroxybutyrate-co-3-hydroxyhexanoate)	For bone regeneration application	Solvent casting method	14.53- 15.32	60 −65	NA	Pore Size $= 414$- $432\,\mu m$	[58, 59]
Macroporous 45S5-polyethylene glycol particles	Tissue Engineering	Sol-gel and pore forming technology	$C_s = 34.4 \pm 5.7$	44.0%	700	Pore size $= 50$- $200\,\mu m$	[60]
45S5 NPs - polycaprolactone	Maxillofacial, craniofacial and periodontal applications	Coagulation, compression moulding and salt leaching technique	$C_s = 36.4 \pm 1.4$	$80.7 \pm 2.3\%$	NA	Young's modulus $= 36.4 \pm 1.4$ MPa	[61]
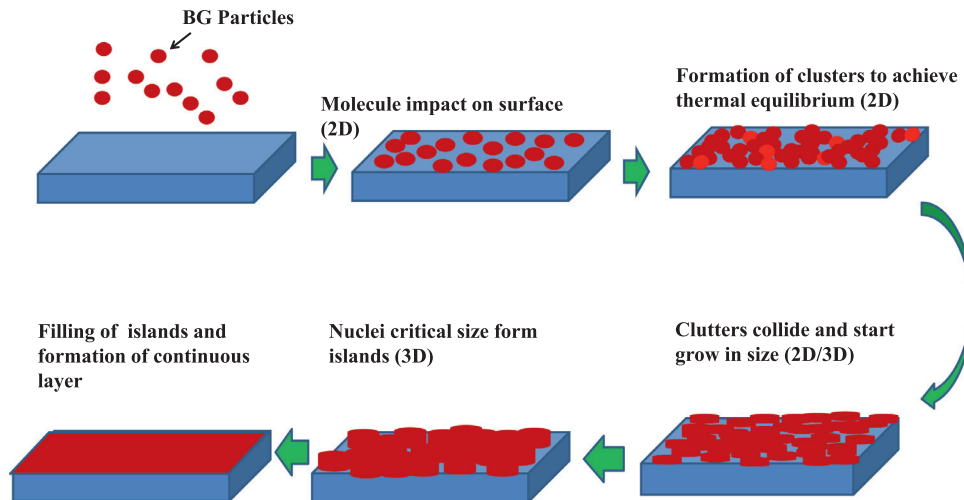
Fig. 4. Step by Step process of thin film deposition.

ties [41–43]. Polymer with BG advanced both biological and mechanical features as listed in Table 1. BG and polycaprolactone composite resulted in improved hardness for tissue engineering application along with good osteoconductive factor [44].

3. Various surface coating techniques for an implant

For long term *in-vivo* application of implant, surface-bone interactions and osseointegration play an important role. It is evidently proven that the enhanced osseointegration is directly correlated with the longevity and biocompatibility of a biomaterial [62], which can be tuned by varying surface properties. Therefore, surface modification or coating of an implant biomaterial is required. Surface modification is found to tune surface chemistry, wettability, charge and roughness, which in turn regulate interfacial and cell-surface interactions [4,63–65]. There are several techniques available for the coating of an implant, which are broadly classified into two categories; physical and chemical [66]. For a particular application, there have been sound arguments in choosing in between these methods. One of the important physical features in both physical and chemical processes is the uniform film thickness, which typically depends on the coating mechanism opted. Coating thickness less than $0.1\,\mu m$ is referred as thin film coating, whereas thickness more than $10\,\mu m$ is referred as thick film [67,68]. During the formation of thin film layer on the substrate, nucleation and growth process occur simultaneously. Detailed step by step formations of the thin film has been explained below in the flow chart Fig. 4. Further, various physical and chemical techniques are briefly outlined in the next section.

3.1. Physical techniques

Physical techniques of film deposition are widely used in semiconductor, aerospace and biomedical industries, and are in high demand mainly for visual/esthetic upgrading, tribolog-

ical behaviour improvement and optical enhancement. They have also been used with chemical techniques to improve thermal properties, increase life span and decrease friction properties [69]. Different physical techniques like spraying, sputtering and laser desperation are discussed in the following sections.

3.1.1. Plasma spraying (PS)

Plasma spraying [70] is divided into two different processes based on the working environments. The first process is conducted under atmospheric conditions and referred as Arc plasma spraying process (APS). Whereas low-pressure vacuum chamber (a protective environment) is also used for PS and referred as Vacuum Plasma Spraying (VPS) or Low-Pressure Plasma Spraying (LPPS) Fig. 5. shows the illustrative representation of a plasma spraying process [71]. It consists of metallic anode and cathode at its gun. High voltage discharge in the presence of non-reactive plasma gas (nitrogen, argon, helium, hydrogen) causes localized ionization [72]. Resistance heating causes the plasma to reach an extreme temperature (10,000–20,000 °C). When the plasma is prepared for spray, the produced arc encompasses down to nozzle and spreads all over the surface. Non-conductive cold gas around the nozzle is used to control the plasma arc velocity and surrounding temperature. The target material is fed to external port near the anode nozzle, which gets rapidly heated and spewed at a distance of 25–150 mm. PS has advantages to spray the high melting point materials i.e. titanium, stainless steel, tungsten, zirconia and aluminium. This technique generally produces a clean, strong and denser coating, which justifies its use for a wide range of applications. The disadvantages of this process are its high cost and complexity.

3.1.2. Sputtering deposition

This process occurs in a low vacuum (0.07–16 Pa) in the presence of inert gas (usually Ar) as shown in Fig. 6. A high voltage (1–5 KV) is applied between the target (made of the sputtered material) and the substrate to be coated. Due to the
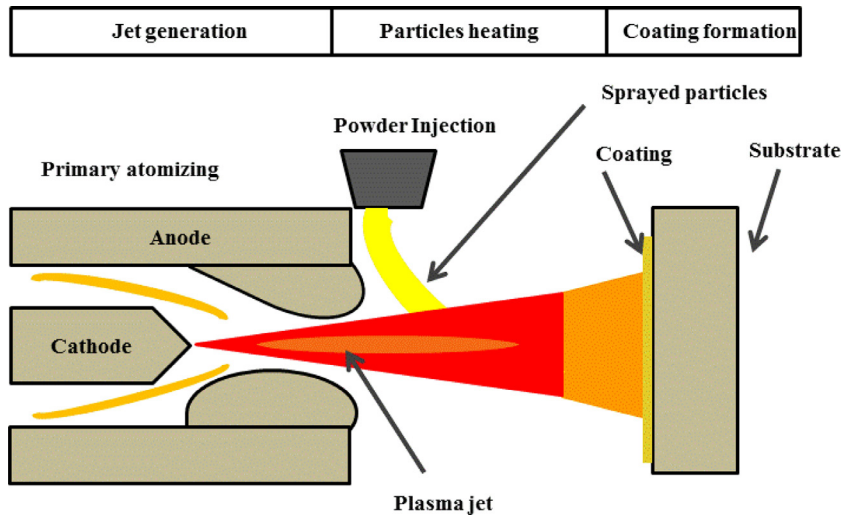
Fig. 5. Diagrammatic representation of the plasma spraying process.
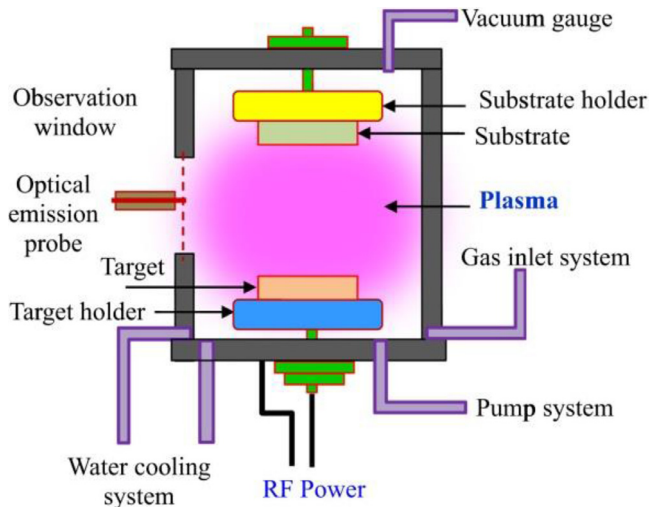
Fig. 6. A schematic representation of a sputtering depositions technique.

high voltage, the inert gas atoms ionize and form a plasma cloud near the surface of the sputtered material. The ions accelerate in the electric field between the substrate and the target material [73]. Sputtered material is bombarded by accelerated inert gas ions from a plasma cloud, which is situated close to the substrate. As a result, atoms and atomic layers are extracted from the sputtered material and then directed to the substrate. It has a number of advantages such as diffused spreading, uniformly coating to a larger area and around corners, low temperature operation and coating of even organic compounds [74].

Another sputtering technique uses magnetron plasma and refereed as Magnetron sputtering (MS). MS is a thin-film physical vapor deposition (PVD) technique and comparably more favorable than various other sputtering techniques available. Its deposition rate is ten times faster than sputtering deposition and causes a lower substrate heating. Both DC and AC sources can be applied for MS and refereed as DC and

RF MS, respectively. It also offers excellent adhesion on the substrate and can simply coat on complex and difficult parts [75,76]. Generally, a high current low voltage strikes at the target made of the material of the future coating. Due to arc striking, a highly energetic emitting zone called as cathode spot appears on the target surface. The temperature inside the cathode spot is around 15,000 °C, causing the evaporation of the target material with the formation of a highly ionized quasi-plasma cloud. The quasi-plasma cloud is directed towards the substrate and deposited by forming a film. Here this coating can be further modified by introducing another reactive gas after the coating, so that gas molecules react with the deposited film and get coated [77].

3.1.3. High velocity oxygen fuel spraying (HVOF)

In HVOF, oxygen and fuel are combined to generate heat and high-velocity particles. Compared to other spraying processes, HVOF has lower flame temperature in range 2500 to 3000 °C causing better density and adhesion of the coating [62]. Uniform and high-density coating is achieved through high-velocity particles collision on the substrate surface, forming a number of compressed plates. Moreover, this technique is capable of producing a high bond strength in the range of 20 to 70 MPa [78]. However, sometimes increase in temperature induced by the collisions causes the transformation of the surface [79].

3.1.4. Pulsed laser deposition (PLD)

PLD using pulsed exciter laser source under vacuums at a pressure of 10^{-4} Pa is used to dissipate energy by melting the target. In PLD, the pulse of laser energy removes (evaporates) the material from the target. This vaporized material containing ion, electrons etc. known as plasma plume expands on the substrate surface. Film growth occurs on the surface because of the re-condensation of plume material [76, 80]. The deposited film is then annealed to attain its crystallinity. The thickness of the coating obtained through this

process lies between 0.5 to 5 μm at room temperature. PLD process works in a range of temperature from 400 to 800 °C. It has several advantages like enhanced film quality, excellent transfer of stoichiometry between the target and the film. However, the splash effects, which involve the production of micro-particles, result in a poor film quality [81].

3.2. Chemical techniques

Chemical techniques involve transport of precursors to vapors phase in the chamber to be condensed on a substrate. Various chemical disposition techniques such as sol-gel, biomimetic and electrophoretic deposition are discussed in the following sections.

3.2.1. Sol-Gel deposition

The Sol-Gel deposition is a widely used chemical method for the coating comprising hydrolysis, condensation and drying processes. Hydrolysis is a rapid process that produces metal hydroxides, which condense to form a three-dimensional gel. This gel is dried to achieve the final deposition. The liquid phase from the gel is removed by gas or evaporation and the resulting gel is refereed as Aerogel or Xerogel, respectively [82–84]. Further, this method is classified into Aqueous Sol-Gel (Asg) and Non-aqueous Sol-Gel (NAsg) methods. In Asg, oxygen provided by the solvent [85] is required to form a layer of metal oxide. Whereas in the case of NAsg, oxygen for the formation of metal oxide is provided from the non-aqueous solvents (ketones, alcohols, aldehydes). These organic solvents apart from providing oxygen also play an essential role in affecting key surface components like morphology, composition of oxide materials, and particle size [86]. Though sol-gel method have a number of advantages such as coating of intricate shapes, low processing temperature and less impurity [87]. But the poor interface, coating defects and a longer period of processing are also derived in this technique.

3.2.2. Biomimetic deposition

The biomimetic deposition is a synthetic deposition in which similar environments of human body condition are created to perform a biochemical reaction. In general simulated body fluid (SBF) at body temperature 37 °C is used to create the environment [88]. Importantly various other coatings, for example, PS, sputtering deposition, PLD and HVOF are performed in the environment other than their applications, which results in poor stability or rapid release of coating to the environment. After eliminating this drawback, biomimetic deposition is also found to enhance the metal biocompatibility and bioactivity. This method involves instant nucleation and growth for the formation of the coating. Its application involves increasing the biomimetic levels from chemical composition, structural organization, morphology, nanostructure, and mechanical behavior. This process continues until the chemical and physical properties of a surface become bioactive and stimulates cellular materials.
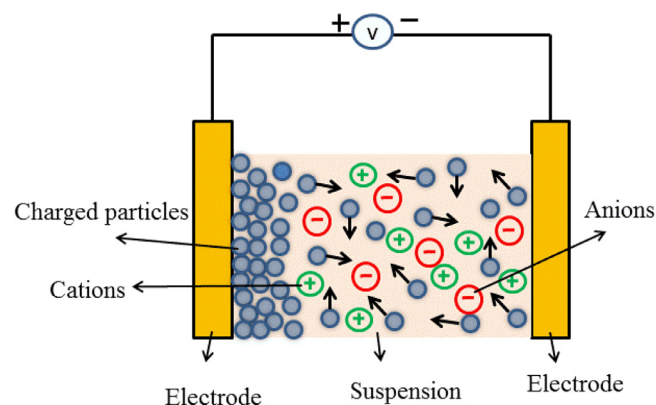
Fig. 7. Schematic of the electrophoretic deposition process.

3.2.3. Electrophoretic deposition

Electrophoretic deposition (EPD) is a low cost electrochemical process in which particles suspended in a solution get charged due to the applied electric field as shown in Fig. 7. These charged particles get collected on one of the electrodes and form a coherent deposition of similar shape levied by the electrode [89]. It is used for the deposition of a variety of materials, such as polymer, composites and biological entities [90,91]. EPD has a number of advantages than other chemical processes like it allows various substrate shapes, has simple apparatus and very short deposition time. It has limitation to work only for conductive substrates and requires heating after deposition to increase the coating density.

Though a number of processes are available for coating of the thin film field but physical processes like plasma spraying, HVOF and chemical processes such as biomimetic yet to be explored for deposition on magnesium alloys. It has been observed that in the case of magnesium alloys high temperature deposition techniques have limitations. As working temperature for magnesium alloy is low (≤400 °C), which limits its use for high temperature processes. These processes like sol-gel and electrophoretic have advantages over others. Also, physical methods like sputtering under vacuum on magnesium alloys need to be explored in this regard. Next section covers the recent advances, in the BG deposition on magnesium alloys from available processes. Detailed comparisons of technique available have been shown in Table 2.

4. Coating of bioactive glass on magnesium alloys

For enhancing the osseointegration of metallic implants, nowadays many researchers have tried to apply appropriate surface reactive materials [4,101]. These reactive materials have been studied in the long run for enabling better bioactivity and tissue response. Some of the frequently used reactive materials for an implant are calcium phosphates (CaP), beta-tricalcium phosphate (β-TCP), biphasic calcium phosphate (BCaP) as hydroxyapatite (HAP), polyether ether ketone, nano-diamonds, and 45S5 bioactive glass-ceramics. These reactive materials have helped in producing an implant material with better cell response, strength and corrosion

Table 2
Comparison of different physical and chemical deposition on implant surfaces.

Techniques	Targets	Maximum coating temperature	Thickness range (μm)	Rate of disposition	Ref.
Physical deposition technique					
Plasma Spraying	Control wear behavior of Al alloy and Mild-steel	20,000	100–300	Fast	[92,93]
Sputtering deposition	Uniform, Non porous, hard durable coating	400–600	0.2–25	Slow	[94,95]
HVOF	Attain maximum hardness, minimum porosity and high temperature corrosion resistance	2500–3000	300–350	Medium	[96,97]
PLD	To attain high chemical resistant and mechanical stable coating	650	0.2–0.5	Fast	[98]
Chemical deposition technique					
Sol-gel Deposition	Biocompatible and less degradable coating for Biomedical devices and specimens	25–65	0.6 - 2	Slow	[22,84]
Biomimetic deposition	To have good hydrophobicity, high adhesion and thermal stabile deposition	37 - 45	1–30	Medium	[99,100]
Electrophoretic deposition	Cost effective bioceramic composite deposition	25–50	1–500	Fast	[89,90]

resistance. Doping of novel nanomaterials such as Ag, Zn, Cu, Fe in these reactive materials to improve antibacterial, corrosion resistance, and degradability also have been studied by researchers [102–105]. Various examples of comparative BG coatings on magnesium alloys AZ31 is revisited and analyzed.

4.1. Mechanism of corrosion/degradation of AZ31

Corrosion of AZ31 for implant applications is not a new issue and many researchers are working to overcome this. It is mainly due to exposer of AZ31 to salty water, acidic liquids or moisture [106]. To control corrosive behavior pretreatment or coatings of appropriate biomaterials have been looked as a strategy. The corrosion behavior of AZ31 in the saline atmosphere is mainly due to the formation of $Mg(OH)_2$ from precipitation of AZ31 corrosive products. Followings are the step reactions when AZ31 immersed in neutral NaCl solution [107–109].

$$O_2 + 2H_2O + 4e^- \rightarrow 4OH^- \quad [108]$$

$$2H_2O + 2e^- \rightarrow 2OH^- + H_2 \quad [108]$$

$$Mg \rightarrow Mg^{2+} + 2e^- \quad [108]$$

Overall:

$$Mg^{2+} + 2OH^- \rightarrow Mg(OH)_2 \quad [108]$$
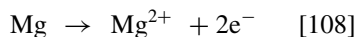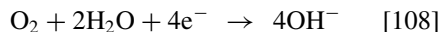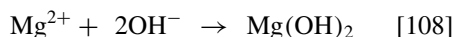
If any modification through pretreatment or coating technique on AZ31 causes an increase in corrosion resistance. It can be understood by a balance between dissolution and formation of $Mg(OH)_2$ and bringing it to a constant thickness value. In this direction, the coatings of BG have been investigated by various groups.

4.2. Sol-gel coating of BG

In a study, Ye et al. [110] coated 45S5 (BG) on AZ31 by a sol-gel dip coating method. Crack free uniform coating thickness of $0.1\,\mu m$ was achieved to impair the corrosion property of AZ31. Immersion test in SBF suggested that crack free 45S5 coating on AZ31 have protected the sample over a period of 7 days. Potentiodynamic polarization test revealed an increase in corrosion resistance by increase in corrosion potential (E_{corr}) value from $-1.60\,V$ for uncoated to $-1.40\,V$ for the coated substrate. Similarly, the same group Huang et al. [111] prepared mesoporous bioactive glass (MBGC) and coated on AZ31 by a sol-gel dip coating method. Pluronic F127 surfactant was used to perform a dual role (depicted in Fig. 8) as a dispersant to get attached on the surface during the sol gel process and thereby agglomerating the particles by reducing the surface tension. It also acted as a template to generate mesoporous structure during the heat treatment stage. In fact, using F127 mesoporous phase on magnesium alloys was achieved at early glass transition temperature of $450\,°C$ than $785\,°C$ [112]. Potentiodynamic polarization test obtained $-1.47\,V$ value for MBGC coated AZ31, which was higher than the uncoated surface of $-1.61\,V$. Water contact angle of coated MBGC was reported around 8° as compared to 70° for uncoated surface. This hydrophilic nature appeared because of the formation of a microtextured surface on MBGC-AZ31, which resulted in an increase in contact surface area. In a similar approach to improve the corrosion resistance of AZ31, coating of bioactive mesoporous 58S bioactive glass (58S MBG) was done [84]. An impressive decrease in the water contact angle of 58S MBG coated to about 14° from 80° of AZ31 sample was reported. It resulted in high surface energy, which in turn enhanced surface adsorption and reaction with Ca^{2+}, PO_4^{3+} and OH^- from SBF [113]. Thereby large amounts of calcium phosphates were formed on the MBG
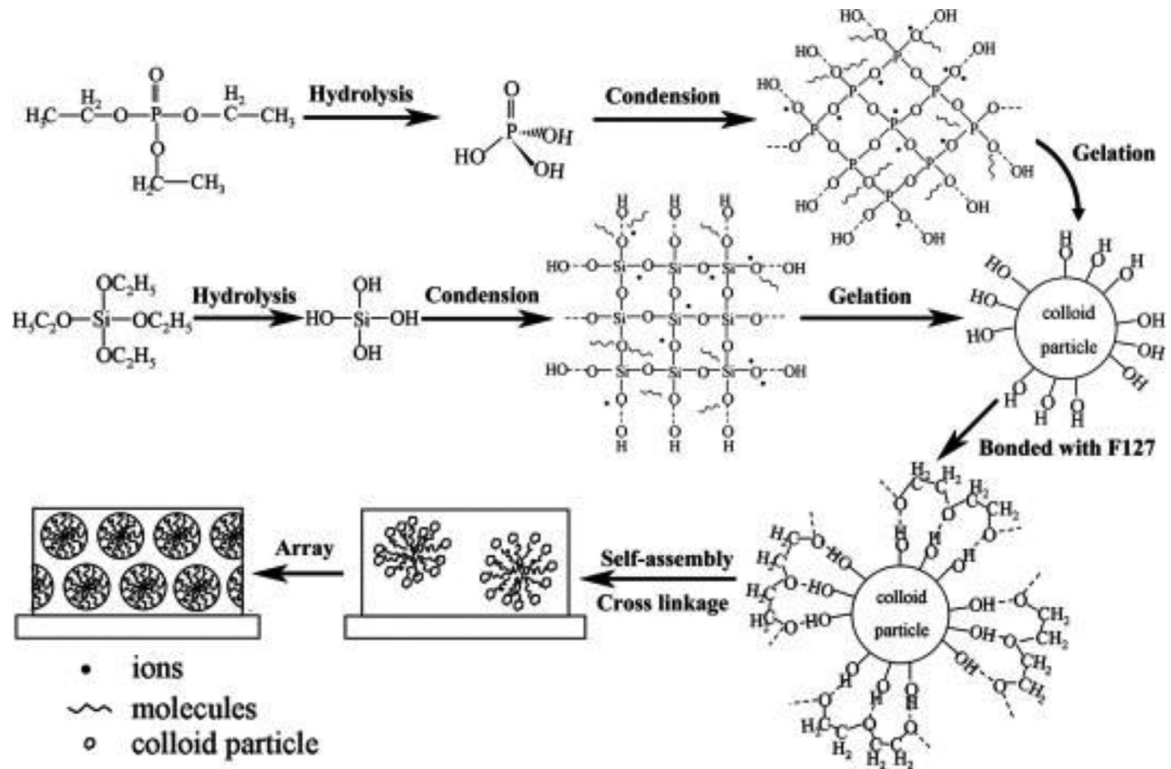
Fig. 8. Role of F127 pluronic surfactant in the preparation of 45S5 MBGC by sol-gel process Adapted with permission from Ref. [84].

surface. When tested in SBF for 14 days, MBG coated sample weight loss was 10% of the original weight whereas the same for the uncoated was 57%.

The effects of processing parameters (conditions) during the coating of 45S5 on AZ31 through a sol-gel dip coating technique were investigated by Dou et al. [22]. These dependent parameters included concentration, duration and withdrawal speed (which predominantly affects density), calcination temperature, layer thickness and porosity [22,114]. Crack free coating thickness of 0.48 to 1 μm of BG coating was achieved. *In-vitro* corrosion properties of this BG coated AZ31 in modified-SBF for different periods were also investigated. Mass loss (%) of different coated samples of varying thickness namely A500 (0.48 μm), 2A500 (0.63 μm) and 3A500 (1 μm) is shown in Fig. 9. Up to 3 days of immersion, all the coated substrates were stable i.e. no significant degradation was observed. However afterwards, a major degradation was detected for the coated samples as well expect 3A500. Only ~2% moss loss was reported for 3A500 in comparison with bare AZ31 (~78%). This indicated a coating thickness of 1 μm is desired to withstand the degradation up to 7 days. In fact, the solution pH was found to be 9.67 and 11.04 in case of 3A500 and other surfaces, respectively. This agreed to the release of Mg(OH)$_2$ during the degradation process and in turn increases in the solution pH [108].

The process of corrosion (degradation) of two different coated surfaces with varying thickness is illustrated in Fig. 10. It can be seen that the crack propagation of A500 (thin coating) was quite easier comparing with 3A500 at 1 day of im-
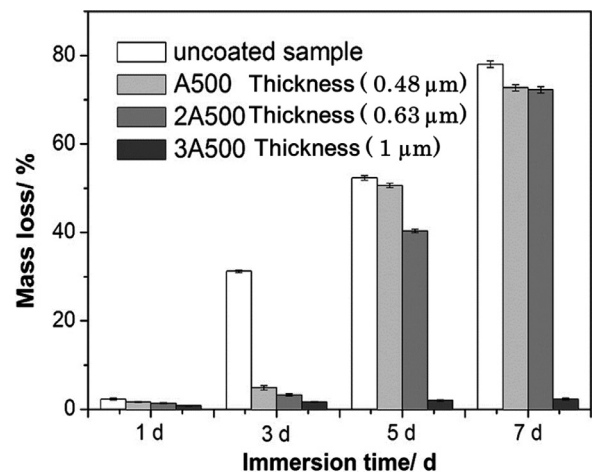
Fig. 9. Percentage mass loss of coated and uncoated AZ31 of varying coating thickness in modified-SBF. Adapted with permission from Ref. [22].

mersion. Thus for A500, crack propagated through the coating within 3 days of immersion, whereas only fewer cracks were observed in case of the thick coating. In continuation, medium permeated to the substrate surface and peeled off of the thin layer coating at 5 days of immersion. This highlighted that coating thickness delayed the formation of cracks, which took a longer time for passing through the coating in case of thick coating and in turn peeling off was evaded. Thereby, the degradation of thick coatings was almost negligible up to 7 days after immersion in SBF.
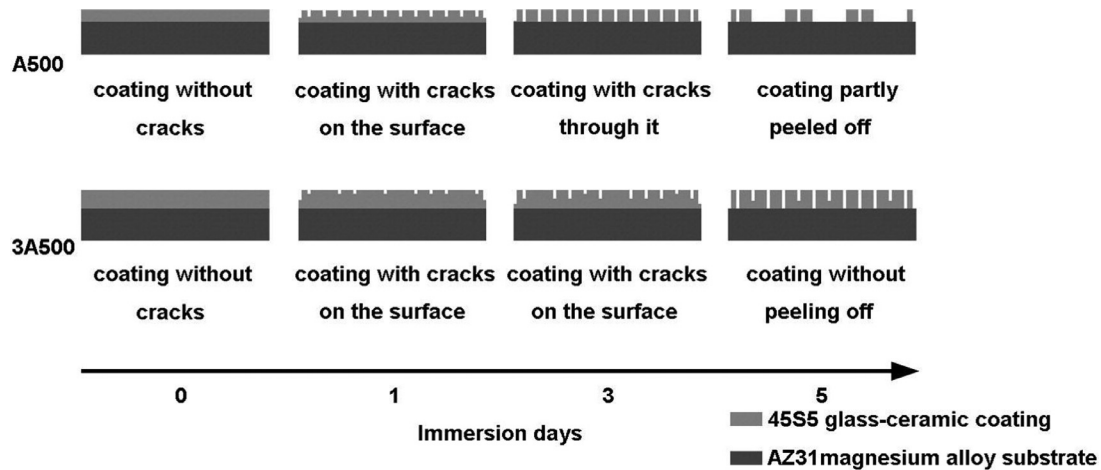
Fig. 10. Schematic illustration of the corrosion process of A500–0.48 μm thick coating and 3A500–1 μm thick coating. Adapted with permission from Ref. [22].

In a work, Zhang et al. [30] studied the effect of different load on MBGC coating on AZ31. Corrosive property obtained from potentiodynamic test analysis, revealed the decrease in the corrosion resistance to -1.76 V (E_{corr}) under load condition as compared to -1.53 V (E_{corr}) for MBGC coated AZ31. Immersion test in SBF for 7 days resulted in the corrosion rate with and without load to be 1.34 mm/y and 0.59 mm/y, respectively. This study revealed that MBGC coating loses its protecting nature completely at a load greater of 25 MPa i.e. at this load the corrosion rate was the same as the uncoated substrate (AZ31).

It is also observed that weak adhesive strength between coating and substrate has impeded the corrosion resistance. The adhesion strength obtained from a sol-gel dip coating on magnesium alloys has been reported to be ~10 MPa, which is considerably below the adhesion strength obtained by conversion coatings on AZ31 as 20 MPa [115]. Also, as per the standard (BS ISO 13,779–2) the minimum bond strength of bioactive coating on metal substrate implant is required to be 15 MPa [116,117]. The heat treatment, phases of coating materials, surface pretreatment and chemical (bonding) interactions are found to influence the adhesion strength [111,118,119]. Shen et al. demonstrated the effects of heat treatment on the tensile bond test for BG sol-gel coated AZ31 at different temperatures (350–500 °C) [119] as shown in Fig. 11. It was reported that at the initial heat treatment of 350 °C the BG remained in the amorphous phase with high porosity and resulted in the poor cohesive strength. After a further increase in the temperature towards glass transition (~400 °C), BG continuously shrank and became less porous. It enhanced the bond strength and the maximum strength of 27.0 ± 2.9 MPa was observed at 450 °C. Additional heat treatment at a higher temperature increased the interfacial residual stress and micro cracks were formed [28]. Consequently, the adhesion strength decreased to 18.1 ± 2.0 MPa [119]. This highlighted that the increase in heat treatment temperature shifted the cohesive bonding towards adhesive bonding.
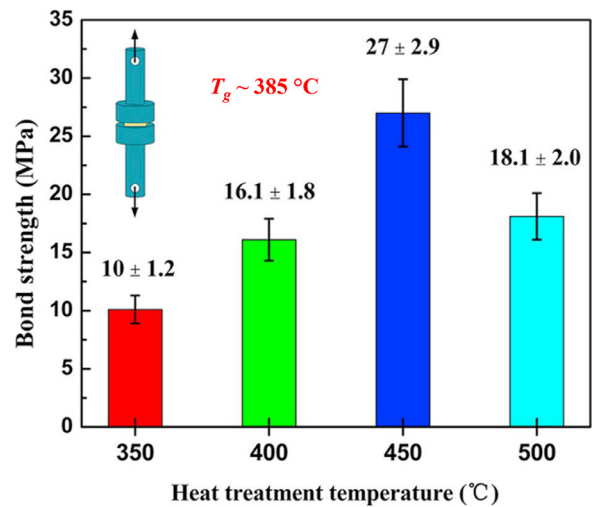
Fig. 11. Correlation between bond strength and heat treatment temperature. Adapted with permission from Ref. [119].

It was understood from the above study that the phases of BG to be coated over the metallic surface affect the adhesion strength. In a separate study, coating of mesoporous BG resulted in the improved adhesion strength than non-mesoporous BG [111]. It is established that the formation of Mg–O–Si bonds between the alkoxide hydroxyl groups (silanols Si–OH) and the metal hydroxyls (MeOH) through a condensation reaction occurs at the interface. The mesoporous BG provided more numbers of silanols than non-mesoporous BG and thus more bodings with the AZ31 contributed to the enhanced adhesion strength [111]. In another study, hydrotalcite particles were doped with the BG to improve adhesion strength and in turn corrosion resistance. Hydrotalcite contains large numbers of interlayer hydroxyls, which contributed to more bond formations with MeOH and enhanced the adhesion strength [120].

Further, researchers have pretreated surfaces to improve BG-surface bonding and achieve better adhesive strength
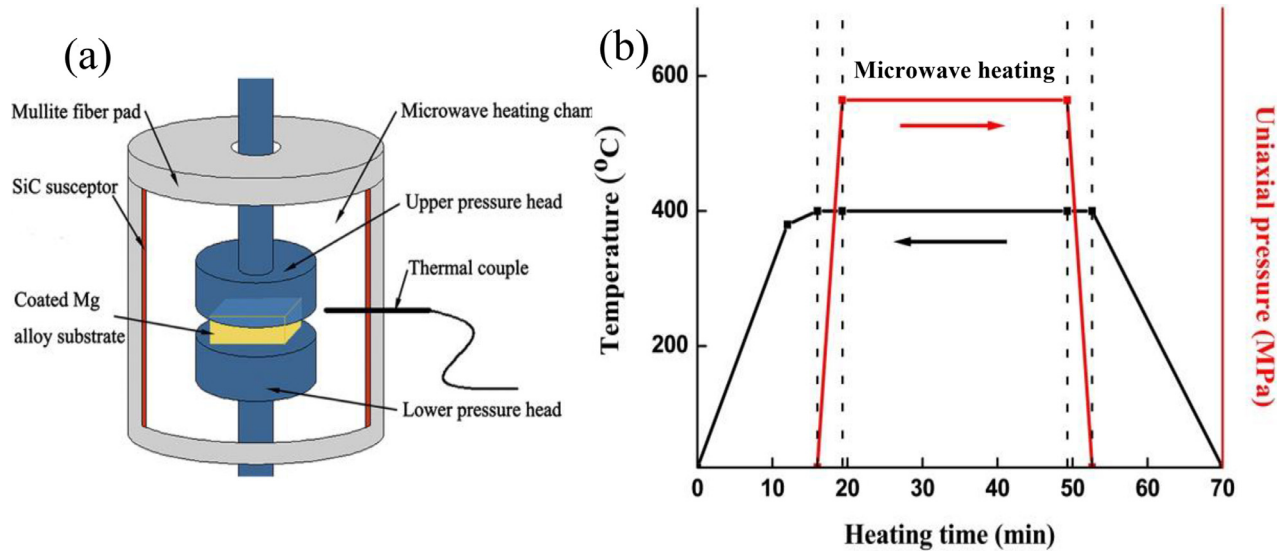
Fig. 12. (a) Uniaxial pressing and microwave hybrid heating chamber (b) Microwave heating ramp rate at uniaxial pressure. Adapted with permission from Ref. [123].

[118,121,122]. Pretreatments of alkali, acid and ionic liquids are reported to improve the adhesive strength and in turn decreased degradation rate of AZ31 [118,122] due to chemical bond formation during the coating. Thus, the exposed surface magnesium hydrates react with silicon hydroxyls of bio-ceramics to form Mg–O–Si bonds. The tensile adhesion strength of an AZ31 sample pretreated with alkali (15 g/l for 60 min) was enhanced to 23.7 ± 2.1 MPa as compared to the untreated one (11.8 ± 1.2 MPa) [118]. The pretreated substrates were more hydrophilic than bare substrate i.e. surface wettability was improved. Further, heat treatment was also found to minimize the surface cracks and further enhanced adhesion strength. After, heat treatment at 500 °C, the adhesion strength of the same sample was increased to 28.5 ± 2.3 MPa. In fact, coating thickness was also increased after heat treatment from $0.90 \mu m$ to $1.30 \mu m$ [118]. In another approach to improve the bond strength and corrosion resistance, Shen et al. [123] coated BG on AZ31 using a unique fabrication method including uniaxial pressing and microwave hybrid heating Fig. 12. Uniaxial pressures of 0, 2, 4 and 6 MPa were applied for 30 min after initial heating up to 400 °C (glass transition temperature). The bond strength increased from 16.1 ± 1.8 MPa at no load to a maximum of 25.8 ± 2.6 MPa at 4 MPa, and further decreased at 6 MPa to 21.0 ± 2.3 MPa.

These behaviors were correlated with surface morphologies of coatings Fig. 13. In the absence of uniaxial pressure, many pores were present on the surface, which decreased remarkably with an increase in loads and the densest coating was obtained at 4 MPa. Thus applied pressure also enhanced the interfacial mechanical interlocking along with the formation of Mg–O–Si bonds and resulted in better adhesion strength. However, at a higher load of 6 MPa, micro-cracks were formed on the surface presumably due to the difference in young modulus between BG (~ 35 GPa) and AZ31

(~ 44 GPa), which caused the generation and accumulation of tensile stress at coating interface. Hence, the bond strength also decreased at a higher load. In fact, corrosion resistance also followed a similar trend as adhesion strength. The corrosion current density (A cm^{-2}), measured using potentiodynamic polarization test in SBF solution, decreased from 5.01×10^{-5} for no load to the minimum value of 7.94×10^{-7} for 4 MPa, and further increased to 2.0×10^{-6} for a higher load of 6 MPa.

4.3. Electrophoretic deposition (EPD) of BG

Rojaee et al. [124] deposited $20 \mu m$ thick BG nano-powder over magnesium alloy through EPD methods using graphite plate as an anode. Two BG derivatives were obtained due to the difference in thermal treatment at 520 °C (BG520) and 1000 °C (BG1000), respectively. BG520 was found to amorphous due to the higher crystallization temperature of BG (545 and 560 °C), BG1000 showed the presence of Wollastonite ($CaSiO_3$) and Cristobalite (SiO_2) crystalline phases (Fig. 14a). Prior to EPD, micro arc oxidation [125] pretreatment was performed in an aqueous saline solution using AZ91 as an anode and a stainless steel plate as a cathode. Colloidal stability analysis showed that isoelectric point ($Z = 0$) for amorphous BG520 at pH 0.8, which was too low for coating on magnesium alloys. Whereas isoelectric point in the case of crystalline BG1000 was pH 4 as shown in Fig. 14b. Similarly, the zeta potential of BG1000 was much higher than BG 520. This indicated suitability of BG1000 coating on magnesium alloys. After deposition, the electrochemical analysis revealed an increase in corrosion potential of BAG/MAO coated AZ91 (-1.32 ± 0.03 V) as compared to pristine AZ91 (-1.45 ± 0.05 V). It was interesting to estimate the degradation rate of BG/MAO coated AZ91 as 2.1×10^{-4} mg cm^{-2} day^{-1}. It is expected that for an implant
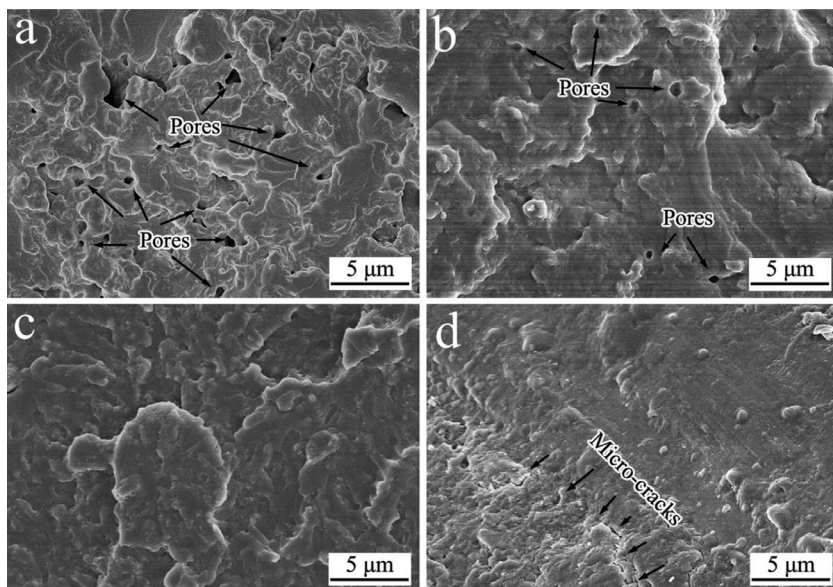
Fig. 13. Surface morphology of Microwave heated uniaxial loaded Bg at (a) 0 MPa pressure (b) 2 MPa pressure (c) 4 MPa pressure (d) 6 MPa pressure. Adapted with permission from Ref. [123].
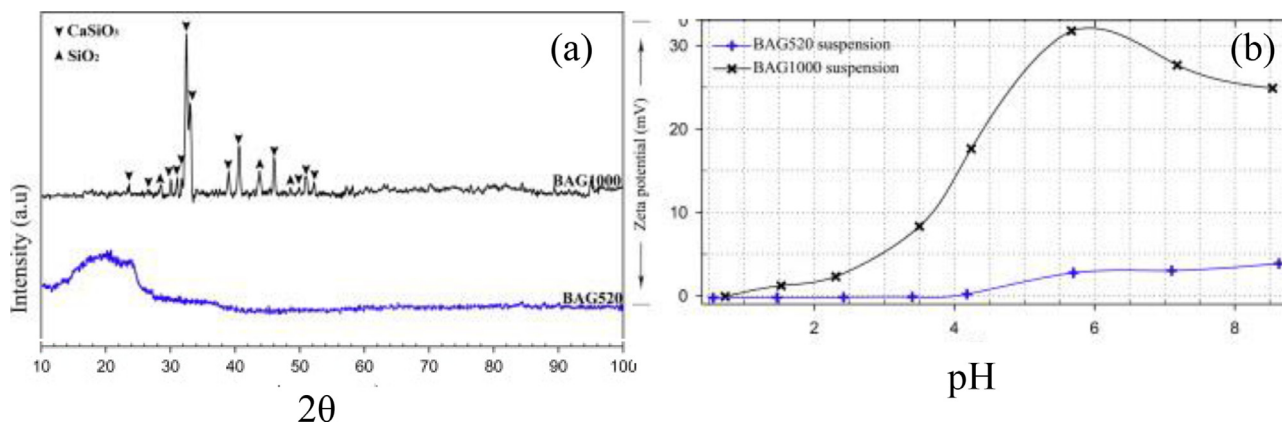
Fig. 14. (a) Phase analysis of BG520 and BG1000 along with (B) Zeta potential and conductivity analysis. Adapted with permission from Ref. [124].

of 10 cm^2 size, daily release of Mg (1.9×10^{-3} mg), Al (1.9×10^{-4} mg) and Zn (2.1×10^{-5} mg) would be under the safe limits of human body daily requirement.

4.4. Coating of BG-polymer composite

Heise et al. [126] investigated the corrosion behavior of chitosan-BG coated magnesium alloy, which was pretreated in Dulbecco's Modified Eagle Medium (DMEM). Stability of a suspension of particles as shown in Fig. 15 were compared between BG in deionized water (DI), BG in DI-ethanol mixture and Chitosan-BG in DI-ethanol mixture. A positive zeta potential ($+42$ mV) in a stable region was reported for Chitosan-BG mixture. It suggested that magnesium alloy to be coated at the cathodic electrode in EPD. The coating thickness of $\sim 2\,\mu$m was achieved. The electrochemical analysis revealed the enhanced impedance for pretreated and coated to ~ 2700 Ohm.cm^2 as compared to double layer coated sam-

ple on untreated magnesium alloys (~ 480 Ohm.cm^2). Surface wettability of bare alloy was around 61°, which decreased to 37° after the coating without pre-treatment. This indicated the presence of relatively higher content of hydrophilic BG than hydrophobic chitosan. While, the contact angle of the DMEM pretreated substrate was 32°, which increased to 51° after the coating presumably due to higher relative content of chitosan. In fact, average roughness (Ra) of the bare alloy ($0.30\,\mu$m) was increased to $0.90\,\mu$m after the pre-treatment. Hence coating roughness, Ra of 1.3 and $2.2\,\mu$m were obtained in case of bare and treated alloy. This suggested that pretreatment of the substrate before disposition controls the degradation rate.

Höhlinger et al. [127] highlighted the protein influence on the degradation of chitosan-BG coated magnesium alloys. Electrophoretic coated magnesium alloy was immersing in the presence and absence of fetal bovine serum (FBS) in DMEM. In the presence of FBS in DMEM, magnesium alloy showed no significant mass loos after 3 days and 7 days of immersion
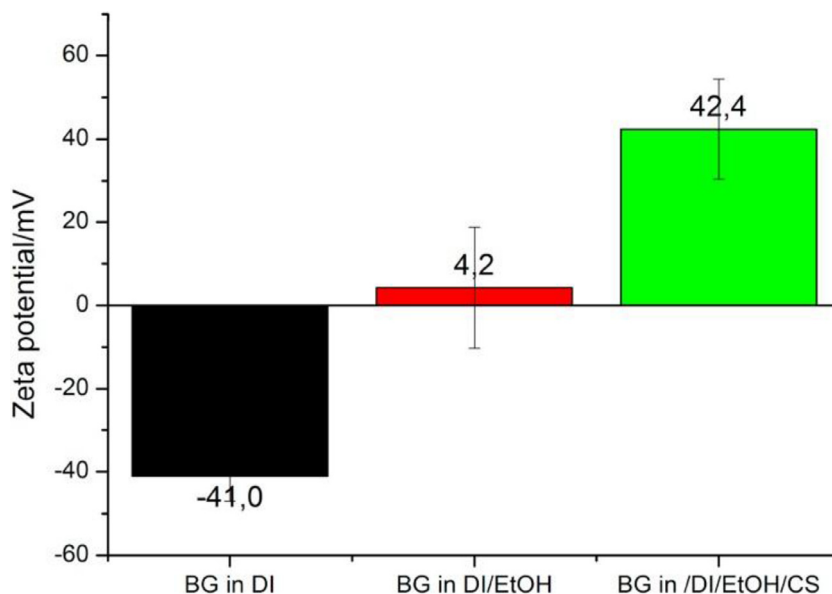
Fig. 15. Zeta potential analysis of BG and Chitosan/BG in different solutions. Adapted with permission from Ref. [126].
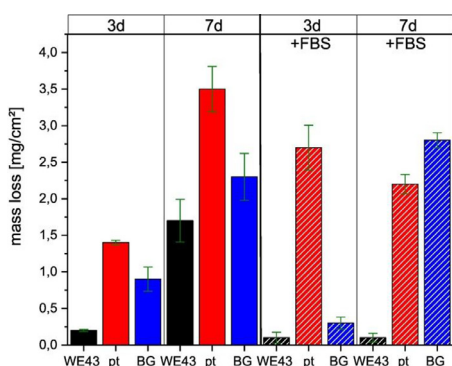
Fig. 16. Mass loss (mg/cm^2) of uncoated, pretreated and coated magnesium alloy immersion in with and without FBS DMEM solution. Adapted with permission from Ref. [127].

as shown below in Fig. 16. But drastic change was observed in case of chitosan-BG coated sample for 7 days, which was comparable to uncoated on 3rd day of immersion. DMEM without serum showed a trend for 3 and 7 days in which the highest mass loss was observed on pretreated (DMEM) followed by chitosan-BG coated and uncoated magnesium alloy. These findings also highlighted the different degradation behaviors of coated AZ31 in SBF, DMEM and DMEM with protein. Hence, the degradation studies should be performed in a suitable medium relevant to a particular application.

In the work, a possible mechanism of degradation of pretreated and chitosan-BG coated sample in FBS-DMEM was also illustrated as shown in Fig. (9). The surface of the pretreated sample results in less protein attachment and weak adhesion to phosphate layer on the surface causing no protective effect in 3 days of immersion. But after 7 days immersion, an increase in protein adhesion hinders the aggressive ions to corrode the surface. Whereas in the case of chitosan-BG coated an opposite phenomenon was observed as shown in

Fig. 17. For 3 days of immersion, chitosan helps in improving the protein adhesion thereby protecting from degradation. Whereas in case of 7 days, left particles of bioactive glass from protein adhesion start getting to dissolve in the solution causing the degradation of the sample.

5. Interfacial aspects of BG coating on AZ31

It had been understood through the literature that before deposition of any film over any substrate for biomedical application, it is significant to have an understanding of important factors affecting the process or performance of bio-material. The implication of various surface and interfacial factors towards coating of BG on AZ31are summarized based on the reported data.

5.1. Surface chemistry

Bio-active glass is a ceramic, which consists of SiO$_2$ ($\sim$50%), Na$_2$O ($\sim$24%), CaO ($\sim$27%), and P$_2$O$_5$ ($\sim$2.60%). Application of BG to the surface of magnesium alloys is directly dependent on the followings:

5.1.1. Composition of BG
All the above mentioned constitutes help in providing strength, bio-inertness and bone bonding capability to BG. Change in the composition alters the properties of BG to a great extent. Adding/doping of metal like silver, copper, zinc though provides a new property for the applications (Table 1) but also alters the basic structure of BG. It is mainly done by compromising the Na$_2$O and calcium concentrations [128].

5.1.2. Pretreatment of BG
Pretreatment with alkali, saline and DMEM improved the surface chemistry to some extent. But an ideal treatment to
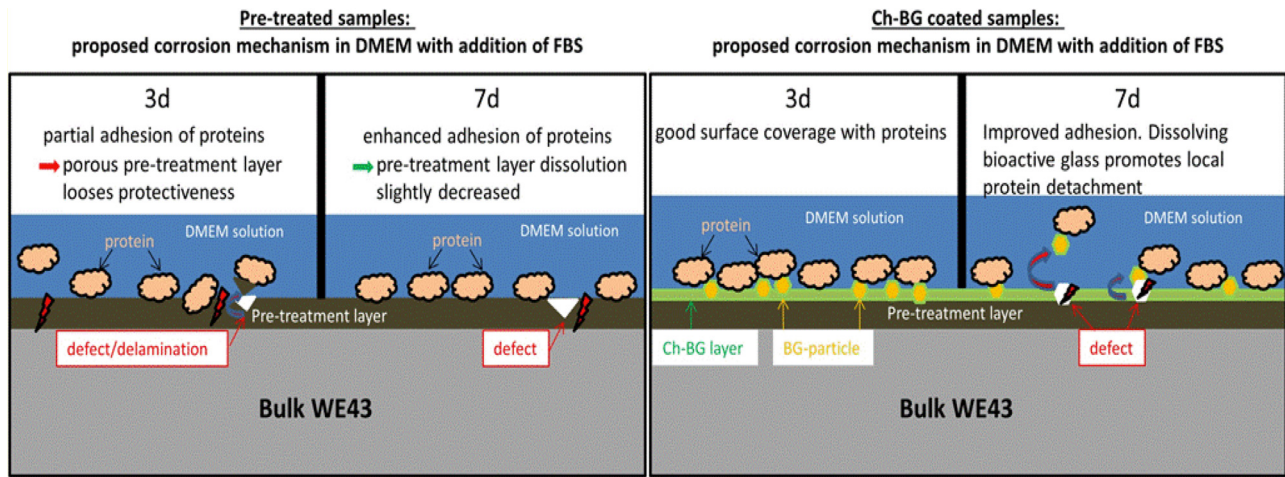
Fig. 17. Illustration of degradation activity of pretreated and chitosan-BG coated for 3 and 7 days Adapted with permission from Ref. [127].
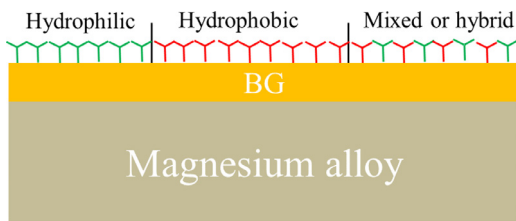
Fig. 18. Different surface functional groups on the BG coated Mg alloys to tune the surface wettability.

Fig. 19. The relation between coating thickness and degradation of coated AZ31.

the surface can be achieved when the release of Mg^{2+} can be utilized to from Mg-O-R, where R is a group of elements that enhances its strength. This also provides the surface to have more options to bond with other substances to improve its properties.

5.2. Contact angle of the coating (Wettability)

Wettability also has an influential role in the interaction between media and bioceramic. It had been noted that coated AZ31 with hydrophilic nature (contact angle $\leq 15°$) resulted in the reduced degradation rate in SBF [110]. Further, the presence of protein in media also affected the degradation behavior due to different adsorption behavior of protein on the surface [127]. In addition for *In-vivo* implant application, the desired wettability is reported in between 50 and 80° [110]. This indicates that the degradation of coated AZ31 can be tuned by controlling the surface wettability for a particular application. The presence of SiO_2 in BG, offers the scope to tune the wettability after coating by functionalization of different groups [4, 63–65,129]. Hydrophilic, hydrophobic or mixed functional groups can be attached to achieve the desired wettability as shown in Fig. 18.

5.3. Young's modulus

Young's modulus of BG is lesser (35 MPa) than AZ31 (44 MPa), which results in poor cohesion between them.

Hence AZ31 should be coated with BG with improved modulus. This can be achieved by doping mental ions or forming composites. The C_s of BG-polymer composites is reported to be enhanced by many folds as listed in Table 1.

5.4. Adhesive strength

A better adhesion between the BG and AZ31 is directly correlated with the good corrosion resistance and the bioactivity of the coated implants. The minimum adhesion required between the BG and AZ31 is 15 MPa [116]. The adhesion strength is dependent on the heat treatment, phases of coating materials, surface pretreatment and chemical (bonding) interactions strength [111,118,119]. The increase in heat treatment temperature regulates the phases of BG, which shifts the cohesive bonding towards adhesive bonding [119]. Mg–O–Si bond formation between BG and AZ31 controls the adhesion strength [111], which is improved by altering the composition of BG, its phases and doping [120]. Similarly, the pretreatment of AZ31 provides more number of surface hydroxyl groups and enhances the bond formations [118,121,122].

5.5. Coating thickness

Optimization of thickness is seen to be an important factor in controlling the degradation rate of AZ31. It had been
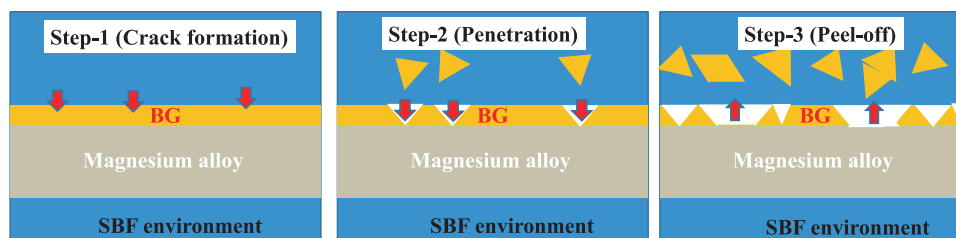
Fig. 20. Schematic illustration of degradation steps of BG coated AZ31 substrate.

observed that low thickness become stable for a shorter duration. Hence a thick coating is required, however, too much thickness builds unnecessary weight. Therefore an optimal thickness of BG should be coated. A typical profile of mass loss vs. coating thickness is depicted in Fig. 19. A thickness of $> 1\,\mu m$ is reported to effectively minimize the degradation behavior of BG coated AZ31 [29].

5.6. Finishing of coating

A typical degradation process of coated magnesium surface is illustrated in below schematic Fig. 20. It is observed that coated surface with some imperfection such as micro-cracks, holes etc. accelerates the rate of corrosion. The main cause for the degradation of the coated AZ31 is the formation of cracks. It begins with the dislocation of the coating particle from some crack region, where SBF solution impregnates into the surface and develops localized corrosion, which ultimately peels out the coating. Hence the finishing of coated AZ31 to eliminate the cracks or pores is essential. It is reported that some thermal or mechanical treatments resulted in the improved finishing of coated AZ31 [123]. Also, the thickness of the coating is reported to regulate the penetration (step-2 of Fig. 19) of the coating.

6. Conclusions

In this review, we have made compiled various literature works done on the coating of BG on Mg alloys to improve its degradation behavior. The physical, chemical and mechanical properties of BG coated Mg alloys are discussed. Synthesis methods, sintering temperature and porosity were found to regulate the properties of the prepared BG. Its compressive strength is inversely related to porosity ad sintering temperature. Further doping of metals to BG and BG-polymers composites also improved mechanical properties. BG is coated on Mg alloys using sol-gel and EPD methods. Underlying interfacial aspects of the coated substrates towards the degradation behavior are highlighted. The degradation rate was found to exponentially decrease with coating thickness and a thickness of $\geq 1\,\mu m$ was reported to be optimal. A hydrophilic coating was found to effective from apatite layer and thus retarded the degradation rate. Surface pretreatment, thermal and mechanical treatments were also reported to influence the adhesion strength and in turn the degradation rate. The crack formation on the coated substrate is the first

step of the degradation process followed by the penetration and peel-off of the coating.

Recent advancements in physical coatings have developed vacuum coatings like sputtering deposition, which can be explored for the coating of BG on Mg alloys. Further, it shall be interesting to see the coating of metal doped BG and its polymer composites towards the degradation behavior. In addition, as the substrate wettability regulates the degradation rate and the presence of SiO_2 in BG allows for the surface medication of coated substrates. Hence the functionalization various groups on the BG coated Mg alloys can be explored to tune the degradation rate.

References

[1] J. Park, R.S. Lakes, Biomaterials: an Introduction, Springer Science & Business Media, 2007.
[2] N. Huang, Y.X. Leng, P.D. Ding, Woodhead Publishing, 2010, pp. 568–602.
[3] S.A. Shaik, K. Bose, H.P. Cherukuri, Mater. Des. 42 (2012) 230–237.
[4] A. Hasan, V. Saxena, L.M. Pandey, Langmuir: ACS J. Surf. Colloids 34 (2018) 3494–3506.
[5] A. Hasan, L.M. Pandey, Appl. Surf. Sci. 505 (2020) 144611.
[6] D. Singh, R. Singh, K. Boparai, I. Farina, L. Feo, A.K. Verma, Compos. Part B: Eng. 132 (2018) 107–114.
[7] R.F. Heary, N. Parvathreddy, S. Sampath, N. Agarwal, J Spine Surg 3 (2017) 163–167.
[8] T.W. Duerig, K. Melton, D. Stöckel, Engineering Aspects of Shape Memory Alloys, Butterworth-Heinemann, 2013.
[9] L. Petrini, F. Migliavacca, J. Metall. 2011 (2011) 501483.
[10] R. Parai, S. Bandyopadhyay-Ghosh, J. Mech. Behav. Biomed. Mater. 96 (2019) 45–52.
[11] C. Zhang, L. Wu, G. Huang, Y. Huang, B. Jiang, A. Atrens, F.-S. Pan, J. Alloys Compd. 823 (2020) 153844.
[12] N. Sezer, Z. Evis, S.M. Kayhan, A. Tahmasebifar, M. Koç, J. Magn. Alloys 6 (2018) 23–43.
[13] R. Radha, D. Sreekanth, J. Magn. Alloys 5 (2017) 286–312.
[14] N. Eliaz, Materials (Basel) 12 (2019) 407.
[15] Y. Liu, S. Zheng, N. Li, H. Guo, Y. Zheng, J. Peng, Sci. Rep. 7 (2017) 40184.
[16] B. Ratna Sunil, T.S. Sampath Kumar, U. Chakkingal, V. Nandakumar, M. Doble, V. Devi Prasad, M. Raghunath, Mater. Sci. Eng. C Mater. Biol. Appl. 59 (2016) 356–367.
[17] D. Bian, J. Deng, N. Li, X. Chu, Y. Liu, W. Li, H. Cai, P. Xiu, Y. Zhang, Z. Guan, Y. Zheng, Y. Kou, B. Jiang, R. Chen, ACS Appl. Mater. Interfaces 10 (2018) 4394–4408.
[18] N.T. Kirkland, Sci. Technol. 47 (2012) 322–328.
[19] L.D. McCabe, B.R. Martin, G.P. McCabe, C.C. Johnston, C.M. Weaver, M. Peacock, Am. J. Clin. Nutr. 80 (2004) 1066–1074.
[20] J.W. Erdman Jr., I.A. MacDonald, S.H. Zeisel, Present Knowledge in Nutrition, John Wiley & Sons, 2012.
[21] N.-E.L. Saris, E. Mervaala, H. Karppanen, J.A. Khawaja, A. Lewenstam, Clin. Chim. Acta 294 (2000) 1–26.

[22] Y. Dou, S. Cai, X. Ye, G. Xu, K. Huang, X. Wang, M. Ren, Surf. Coat. Technol. 228 (2013) 154–161.

[23] F. Witte, N. Hort, C. Vogt, S. Cohen, K.U. Kainer, R. Willumeit, F. Feyerabend, Curr. Opin. Solid State Mater. Sci. 12 (2008) 63–72.

[24] H. Liu, D. Li, Y. Zhang, M. Li, Histochem. Cell Biol. 149 (2018) 393–404.

[25] F. Witte, V. Kaese, H. Haferkamp, E. Switzer, A. Meyer-Lindenberg, C. Wirth, H. Windhagen, Biomaterials 26 (2005) 3557–3563.

[26] M. Haghshenas, J. Magn. Alloys 5 (2017) 189–201.

[27] J.G. Acheson, S. McKillop, P. Lemoine, A.R. Boyd, B.J. Meenan, Materialia 6 (2019) 100291.

[28] C. Mardare, A. Mardare, J. Fernandes, E. Joanni, S. Pina, M. Fernandes, R. Correia, J. Eur. Ceram. Soc. 23 (2003) 1027–1030.

[29] C. Garcia, S. Ceré, A. Durán, J. Non Cryst. Solids 348 (2004) 218–224.

[30] F. Zhang, S. Cai, G. Xu, S. Shen, Y. Li, M. Zhang, X. Wu, J. Mech. Behav. Biomed. Mater. 56 (2016) 146–155.

[31] S.A. Omar, Y. Castro, J. Ballarre, W.H. Schreiner, A. Durán, S.M. Ceré, Corrosion 73 (2017) 1448–1460.

[32] B. Thavornyutikarn, B. Feltis, P.F. Wright, T.W. Turney, Mater. Sci. Eng.: C 97 (2019) 188–197.

[33] J.R. Jones, L.M. Ehrenfried, L.L. Hench, Biomaterials 27 (2006) 964–973.

[34] C. Shuai, J. Deng, C. Gao, P. Feng, S. Peng, T. Xiao, Y. Deng, J. Alloys Compd. 636 (2015) 341–347.

[35] P. Feng, P. Wei, C. Shuai, S. Peng, PLoS One 9 (2014) e87755.

[36] L. Finney, S. Vogt, T. Fukai, D. Glesne, Clin. Exp. Pharmacol. Physiol. 36 (2009) 88–94.

[37] C. Gérard, L.-J. Bordeleau, J. Barralet, C.J. Doillon, Biomaterials 31 (2010) 824–831.

[38] J.R. Jones, L.M. Ehrenfried, P. Saravanapavan, L.L. Hench, J. Mater. Sci. Mater. Med. 17 (2006) 989–996.

[39] M. Kaczmarek, M. Jurczyk, B. Rubis, A. Banaszak, A. Kolecka, A. Paszel, K. Jurczyk, M. Murias, J. Sikora, M. Jurczyk, J. Biomed. Mater. Res. Part A: Off. J. Soc. Biomater. Jpn. Soc. Biomater. Aust. Soc. Biomater. Korean Soc.Biomater. 102 (2014) 1316–1324.

[40] K. Jurczyk, K. Niespodziana, M. Jurczyk, M. Jurczyk, Mater Des 32 (2011) 2554–2560.

[41] V. Saxena, L.M. Pandey, Mater. Today: Proc. 18 (2019) 1388–1400.

[42] V. Saxena, P. Chandra, L.M. Pandey, Appl. Nanosci. 8 (2018) 1925–1941.

[43] A. Hasan, G. Waibhaw, V. Saxena, L.M. Pandey, Int. J. Biol. Macromol. 111 (2018) 923–934.

[44] P.S.P. Poh, D.W. Hutmacher, B.M. Holzapfel, A.K. Solanki, M.M. Stevens, M.A. Woodruff, Acta Biomater 30 (2016) 319–333.

[45] Q.Z. Chen, I.D. Thompson, A.R. Boccaccini, Biomaterials 27 (2006) 2414–2425.

[46] X. Liu, M.N. Rahaman, G.E. Hilmas, B.S. Bal, Acta Biomater 9 (2013) 7025–7034.

[47] F. Baino, E. Fiume, Mater. Lett. 245 (2019) 14–17.

[48] E.A. Aguilar-Reyes, C.A. León-Patiño, B. Jacinto-Diaz, L.-P. Lefebvre, J. Am. Ceram. Soc. 95 (2012) 3776–3780.

[49] S.-C. Wu, H.-C. Hsu, S.-H. Hsiao, W.-F. Ho, J. Mater. Sci. Mater. Med. 20 (2009) 1229–1236.

[50] J. Barberi, A. Nommeots-Nomm, E. Fiume, E. Verné, J. Massera, F. Baino, Biomed. Glasses 5 (2019) 140–147.

[51] B. Thavornyutikarn, P. Tesavibul, K. Sitthiseripratip, N. Chatarapanich, B. Feltis, P.F.A. Wright, T.W. Turney, Mater. Sci. Eng.: C 75 (2017) 1281–1288.

[52] J.H. Lopes, J.A. Magalhães, R.F. Gouveia, C.A. Bertran, M. Motisuke, S.E.A. Camargo, E.d.S. Trichês, J. Mech. Behav. Biomed. Mater. 62 (2016) 10–23.

[53] A. Hoppe, R. Meszaros, C. Stähli, S. Romeis, J. Schmidt, W. Peukert, B. Marelli, S.N. Nazhat, L. Wondraczek, J. Lao, J. Mater. Chem. B 1 (2013) 5659–5674.

[54] W. Guo, F. Zhao, Y. Wang, J. Tang, X. Chen, J. Mech. Behav. Biomed. Mater. 68 (2017) 8–15.

[55] K. Jurczyk, G. Adamek, M. Kubicka, J. Jakubowicz, M. Jurczyk, Materials 8 (2015) 1398–1412.

[56] W. Li, Y. Ding, S. Yu, Q. Yao, A.R. Boccaccini, ACS Appl. Mater. Interfaces 7 (2015) 20845–20854.

[57] Z. Hong, R.L. Reis, J.F. Mano, Acta Biomater. 4 (2008) 1297–1306.

[58] S. Yang, J. Wang, L. Tang, H. Ao, H. Tan, T. Tang, C. Liu, Colloids Surf. B 116 (2014) 72–80.

[59] C. Wu, Y. Ramaswamy, Y. Zhu, R. Zheng, R. Appleyard, A. Howard, H. Zreiqat, Biomaterials 30 (2009) 2199–2208.

[60] N. Li, Q. Jie, S. Zhu, R. Wang, Mater. Lett. 58 (2004) 2747–2750.

[61] P.S. Poh, D.W. Hutmacher, B.M. Holzapfel, A.K. Solanki, M.M. Stevens, M.A. Woodruff, Acta Biomater. 30 (2016) 319–333.

[62] M.S. Zafar, I. Farooq, M. Awais, S. Najeeb, Z. Khurshid, S. Zohaib, Bioactive Surface Coatings for Enhancing Osseointegration of Dental Implants, In Biomedical, therapeutic and clinical applications of bioactive glasses, Woodhead Publishing, 2019, pp. 313–329.

[63] L.M. Pandey, S.K. Pattanayek, Appl. Surf. Sci. 257 (2011) 4731–4737.

[64] L.M. Pandey, S.K. Pattanayek, J. Chem. Eng. Data 58 (2013) 3440–3446.

[65] L.M. Pandey, S.K. Pattanayek, D. Delabouglise, Jo. Phys. Chem. C 117 (2013) 6151–6160.

[66] Z.-Z. Yin, W.-C. Qi, R.-C. Zeng, X.-B. Chen, C.-D. Gu, S.-K. Guan, Y.-F. Zheng, J. Magn. Alloys 8 (2020) 42–65.

[67] A. Das, A.K. Chikkala, G.P. Bharti, R.R. Behera, R.S. Mamilla, A. Khare, P. Dobbidi, J. Alloys. Compd. 739 (2018) 729–736.

[68] T. Zheng, Y. Hu, F.-S. Pan, Y. Zhang, A. Tang, J. Magn. Alloys 7 (2019) 193–202.

[69] R.R. Behera, A. Hasan, M.R. Sankar, L.M. Pandey, Surf. Coat. Technol. 352 (2018) 420–436.

[70] H. Xiao, L. Yan, E.M. Dempsey, W. Song, R. Qi, W. Li, Y. Huang, X. Jing, D. Zhou, J. Ding, Prog. Polym. Sci. 87 (2018) 70–106.

[71] P.H. Li, P.K. Chu, Woodhead Publishing, 2016, pp. 3–28.

[72] D. Thirumalaikumarasamy, V. Balasubramanian, S. Sree Sabari, J. Magn. Alloys 5 (2017) 133–145.

[73] D. Depla, S. Mahieu, J.E. Greene, (3rd ed.), William Andrew Publishing, Boston, 2010, pp. 253–296.

[74] A. Sarangan, Woodhead Publishing, 2016, pp. 149–184.

[75] Z. Cao, Woodhead Publishing, 2011, pp. 185–210.

[76] A. Michelmore, Woodhead Publishing, 2016, pp. 29–47.

[77] M.M. Hassan, Elsevier, 2018, pp. 321–355.

[78] Y.Y. Wang, C.J. Li, A. Ohmori, Surf. Coat. Technol. 200 (2006) 2923–2928.

[79] D. Tejero-Martin, M. Rezvani Rad, A. McDonald, T. Hussain, J. Therm. Spray Technol. 28 (2019) 598–644.

[80] S.M. Best, P.C. Marti, Woodhead Publishing, 2012, pp. 43–74.

[81] J. Pou, F. Lusquiños, R. Comesaña, M. Boutinguiza, Woodhead Publishing, 2010, pp. 394–425.

[82] F. Baino, E. Fiume, M. Miola, F. Leone, B. Onida, E. Verné, Mater. Lett. 235 (2019) 207–211.

[83] Q.Z. Chen, Y. Li, L.Y. Jin, J.M. Quinn, P.A. Komesaroff, Acta Biomater. 6 (2010) 4143–4153.

[84] K. Huang, S. Cai, G. Xu, M. Ren, X. Wang, R. Zhang, S. Niu, H. Zhao, Surf. Coat. Technol. 240 (2014) 137–144.

[85] Y. Jang, D. Owuor, J. Waterman, L. White, B. Collins, J. Sankar, T. Gilbert, Y. Yun, Materials 7 (2014) 5866–5882.

[86] I. Khan, K. Saeed, I. Khan, Arab. J. Chem. **12**, (2017) 908–931.

[87] L.M. Muresan, Intelligent Coatings for Corrosion Control, Elsevier, 2015, pp. 585–602.

[88] F. Liu, J. Xu, F. Wang, L. Zhao, T. Shimizu, Surf. Coat. Technol. 204 (2010) 3294–3299.

[89] R. Rojaee, M. Fathi, K. Raeissi, M.H. Taherian, Ceram. Int. 40 (2014) 7879–7888.

[90] M. Miola, E. Verné, F.E. Ciraldo, L. Cordero-Arias, A.R. Boccaccini, Front .Bioeng. Biotechnol. 3 (2015).

[91] T. Monetta, A. Acquesta, A. Carangelo, N. Donato, F. Bellucci, J. Magn. Alloys 5 (2017) 412–422.

[92] R. Subbiah, A. Arun, A.A. Lakshmi, A. Naga Sai Harika, N. Ram, N. Sateesh, Mater. Today: Proc. 18 (2019) 5151–5157.

[93] C.M. Pavan, M.N. Raj, M. Mahesh Mudhol, B.R. Narendra Babu, Mater. Today: Proc. 27 (2020) 172–176.

[94] D. Liu, H. Ma, Y. Liang, Colloids Surf. B 188 (2020) 110792.

[95] A. Popa, V. Marques, G. Stan, M. Husanu, A. Galca, C. Ghica, D. Tulyaganov, A. Lemos, J. Ferreira, Thin Solid Films 553 (2014) 166–172.

[96] S. Vignesh, K. Shanmugam, V. Balasubramanian, K. Sridhar, Defence Technol. 13 (2017) 101–110.

[97] M. Kaur, H. Singh, S. Prakash, Anti-Corros. Methods Mater. 55 (2008) 86–96.

[98] M. Walczak, E.L. Papadopoulou, M. Sanz, A. Manousaki, J.F. Marco, M. Castillejo, Appl. Surf. Sci. 255 (2009) 5267–5270.

[99] G. Graziani, M. Berni, A. Gambardella, M. De Carolis, M.C. Maltarello, M. Boi, G. Carnevale, M. Bianchi, Mater. Sci. Eng. C 99 (2019) 853–862.

[100] C. Huang, S. Bhagia, N. Hao, X. Meng, L. Liang, Q. Yong, A.J. Ragauskas, RSC Adv. 9 (2019) 5786–5793.

[101] R.R. Behera, A. Das, D. Pamu, L.M. Pandey, M.R. Sankar, J. Mech. Behav. Biomed. Mater. 86 (2018) 143–157.

[102] K. Zhang, B. Zhang, C. Huang, S. Gao, B. Li, R. Cao, J. Cheng, R. Li, Z. Yu, X. Xie, J. Mech. Behav. Biomed. Mater. 100 (2019) 103363.

[103] M. Miola, E. Verné, F.E. Ciraldo, L. Cordero-Arias, A.R. Boccaccini, Front. Bioeng. Biotechnol. 3 (2015) 159.

[104] Y.F. Goh, A.Z. Alshemary, M. Akram, M.R. Abdul Kadir, R. Hussain, Int. J. Appl. Glass Sci. 5 (2014) 255–266.

[105] V.K. Bommala, M.G. Krishna, C.T. Rao, J. Magn. Alloys 7 (2019) 72–79.

[106] G.S. Frankel, A. Samaniego, N. Birbilis, Corros. Sci. 70 (2013) 104–111.

[107] I. Kot, H. Krawiec, J. Solid State Electrochem. 19 (2015) 2379–2390.

[108] Li. Jiang, F. Xu, Zhen Xu, Yu. Chen, X. Zhou, G. Wei, H. Ge, Eng. Fail. Anal. 107 (2020) 104234.

[109] Y. Chai, Y. Song, B. Jiang, J. Fu, Z. Jiang, Q. Yang, H. Sheng, G. Huang, D. Zhang, F.-S. Pan, J. Magn. Alloys 7 (2019) 545–554.

[110] X. Ye, S. Cai, Y. Dou, G. Xu, K. Huang, M. Ren, X. Wang, Appl. Surf. Sci. 259 (2012) 799–805.

[111] K. Huang, S. Cai, G. Xu, X. Ye, Y. Dou, M. Ren, X. Wang, J. Alloys Compd. 580 (2013) 290–297.

[112] C. Duée, F. Désanglois, I. Lebecq, C. Follet-Houttemane, J. Non Cryst. Solids 358 (2012) 1083–1090.

[113] H. Tang, Y. Guo, D. Jia, Y. Zhou, Surf. Coat. Technol. 206 (2011) 8–15.

[114] B.G. Rao, D. Mukherjee, B.M. Reddy, Elsevier, 2017, pp. 1–36.

[115] R. Zhang, S. Cai, G. Xu, H. Zhao, Y. Li, X. Wang, K. Huang, M. Ren, X. Wu, Appl. Surf. Sci. 313 (2014) 896–904.

[116] B. ISO, Implants for Surgery–Hydroxyapatite–Part 2: Coatings of Hydroxyapatite, British Standards Institution, London, UK, 2000.

[117] J. Sun, S. Cai, J. Wei, K.e. Shen, R. Ling, J.e. Sun, J. Liu, G. Xu, Ceram. Int. 46 (2020) 824–832.

[118] H. Zhao, S. Cai, S. Niu, R. Zhang, X. Wu, G. Xu, Z. Ding, Ceram. Int. 41 (2015) 4590–4600.

[119] S. Shen, S. Cai, G. Xu, H. Zhao, S. Niu, R. Zhang, J. Mech. Behav. Biomed. Mater. 45 (2015) 166–174.

[120] D. Álvarez, A. Collazo, M. Hernández, X.R. Nóvoa, C. Pérez, Prog. Org. Coat. 67 (2010) 152–160.

[121] S. Jiang, S. Cai, Y. Lin, X. Bao, R. Ling, D. Xie, J. Sun, J. Wei, G. Xu, J. Alloys Compd. 793 (2019) 202–211.

[122] Y.F. Zhang, B. Hinton, G. Wallace, X. Liu, M. Forsyth, Sci. Technol. 47 (2013) 374–382.

[123] S. Shen, S. Cai, G. Xu, Y. Li, T. Zhang, M. Zhang, Mater. Des. 86 (2015) 610–615.

[124] R. Rojaee, M. Fathi, K. Raeissi, M. Taherian, Ceram. Int. 40 (2014) 7879–7888.

[125] O. Germershaus, S. Mao, J. Sitterberg, U. Bakowsky, T. Kissel, J. Control Rel. 125 (2008) 145–154.

[126] S. Heise, M. Höhlinger, Y.T. Hernández, J.J.P. Palacio, J.A. Rodriquez Ortiz, V. Wagener, S. Virtanen, A.R. Boccaccini, Electrochim. Acta 232 (2017) 456–464.

[127] M. Höhlinger, D. Christa, V. Zimmermann, S. Heise, A.R. Boccaccini, S. Virtanen, Mater. Sci. Eng.: C 100 (2019) 706–714.

[128] A.A. El-Rashidy, G. Waly, A. Gad, A.A. Hashem, P. Balasubramanian, S. Kaya, A.R. Boccaccini, I. Sami, J. Non Cryst. Solids 483 (2018) 26–36.

[129] L.M. Pandey, S.K. Pattanayek, Appl. Surf. Sci. 264 (2013) 832–837.